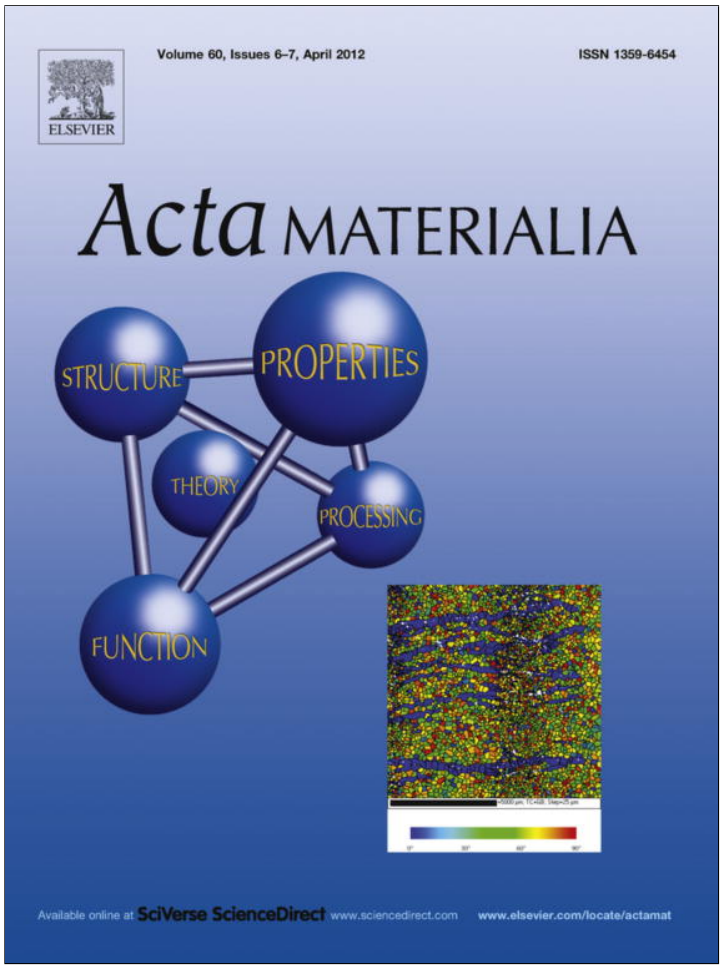

Available online at www.sciencedirect.com
SciVerse ScienceDirect
Acta Materialia 60 (2012) 2873–2885
Acta MATERIALIA
www.elsevier.com/locate/actamat

Mechanical properties of open-cell rhombic dodecahedron cellular structures

Sahab Babaee, Babak Haghpanah Jahromi, Amin Ajdari, Hamid Nayeb-Hashemi, Ashkan Vaziri *

Department of Mechanical and Industrial Engineering, Northeastern University, Boston, MA 02115, USA

Received 12 November 2011; received in revised form 27 January 2012; accepted 28 January 2012
Available online 7 March 2012

Abstract

A series of analytical relationships is presented to predict the mechanical properties and response of open three-dimensional Voronoi tessellation of face-centered cubic structures called rhombic dodecahedrons. The cell edge material was assumed to be elastic–perfectly plastic, and the effective mechanical properties of the cellular structure were related to the cell edge material properties and the relative density of the cellular structure. Detailed finite element models were carried out to establish the validity of the analytical models. In the elastic regime, the monodisperse cellular structure is orthotropic and near-incompressible in all loading directions, and its response is governed by bending deformation of the cell edges. The yield strength of the cellular structure in all loading directions is equal. We also studied the role of irregularity in the organization of the cellular structure on its mechanical properties. The irregularity in the cellular structure organization was introduced by moving the vertices of a regular cellular structure in three orthogonal directions by a random value within a predefined range called the "irregularity index". At a constant overall relative density, increasing the level of irregularity increases the effective elastic modulus and significantly decreases the effective yield strength of the cellular structure. We also studied the mechanical properties of the cellular structure tied to rigid plates, in view of the application of cellular structure as the core construction of sandwich panels. In this case, the cellular structure is significantly stiffer and its mechanical response is dominated by cell wall stretching.

Keywords: Cellular structure; Foam material; Finite elements; Energy methods; Analytic functions

1. Introduction

Three-dimensional cellular materials are ubiquitous in nature and are also used in a variety of engineering applications, ranging from sandwich structures with low-density cores for structural protection [1–6], sound and thermal insulation [7,8], and heat transfer [9–15] to scaffolds for tissue engineering and regenerative medicine [16–18]. In many of these applications, the mechanical properties and structural behavior of the cellular materials play key roles in regulating the overall function of the system. In this context, the mechanics of two-dimensional cellular structures have been studied extensively using theoretical approaches, computational models and robust experiments [19–26]. These studies include investigating the role of structural organization and hierarchy [27–29] and heterogeneity and defects (e.g. missing cell edges or cell clusters) in the behavior of cellular structures [30–37].

Studying the mechanical behavior of three-dimensional cellular structures is inherently more challenging. A limited class of three-dimensional (3-D) base cells (the triangular, rhombic and hexagonal prisms, the rhombic dodecahedron, and the tetrakaidecahedron) can be packed together to generate a monodisperse cellular structure [19,38–41]. The available literature on the mechanics and material properties of 3-D cellular structures is generally focused on the mechanics of tetrakaidecahedral cellular structures,

* Corresponding author. Tel.: +1 617 373 3474.
E-mail address: vaziri@coe.neu.edu (A. Vaziri).

1359-6454/$36.00 © 2012 Acta Materialia Inc. Published by Elsevier Ltd. All rights reserved.
doi:10.1016/j.actamat.2012.01.052

which have a unit cell with six square and eight hexagonal faces [42–44]. The monodisperse open-cell tetrakaidecahedral structures are incompressible cubic materials, with an effective elastic modulus of $\sim 0.63 \times \text{density}^2$ and an ultimate strength of $\sim 0.22 \times \text{density}^{1.5}$ in all basic directions of loading [43–49].

In this work, we studied the mechanical properties of an open-cell rhombic dodecahedron cellular structure. We show that this structure is orthotropic and incompressible, with its material properties being dominated by the bending of the cell edges and having an effective elastic modulus of $\sim \text{density}^2$ in three loading directions. The unit cell of the structure is a space-filling convex polyhedron called a rhombic dodecahedron (also called a rhomboidal dodecahedron). The unit cell of the structure is shown in Fig. 1a, and has 12 identical rhombic faces with 24 edges and 14 vertices. Each face of a rhombic dodecahedron is a rhombus, with angles of $2\alpha = 2\cot^{-1}\sqrt{2} \approx 70.53^\circ$ and $2\theta = \tan^{-1}\sqrt{2} \approx 109.47^\circ$. The volume of a unit cell is $V = 16L^3/3\sqrt{3}$, where L is the edge length. For a square cell edge cross-sectional area, $b \times b$, the relative density (volume fraction) of the rhombic dodecahedron unit cells is $\rho_u = 24b^2L/V = 9\sqrt{3}b^2/2L^2$. For a 3-D rhombic dodecahedron cellular structure of infinite size, each cell edge is shared by three adjacent unit cells, so the effective relative density of a 3-D tessellated cellular structure, denoted by ρ, is $\rho = \rho_u/3 = 3\sqrt{3}b^2/2L^2$. Fig. 1c shows an example of a rhombic dodecahedron cellular structure obtained by packing 66 rhombic dodecahedron unit cells, which has 864 identical cell edges. This monodisperse structure is the Voronoi tessellation of the face-centered cubic lattice (i.e. the Voronoi tessellation of a face-centered cubic lattice gives rhombic dodecahedron cellular structures). In the coordinate system shown in Fig. 1, axes 2 and 3 are perpendicular and normal to the top and front surfaces of rhombic dodecahedron in the outward direction, respectively.

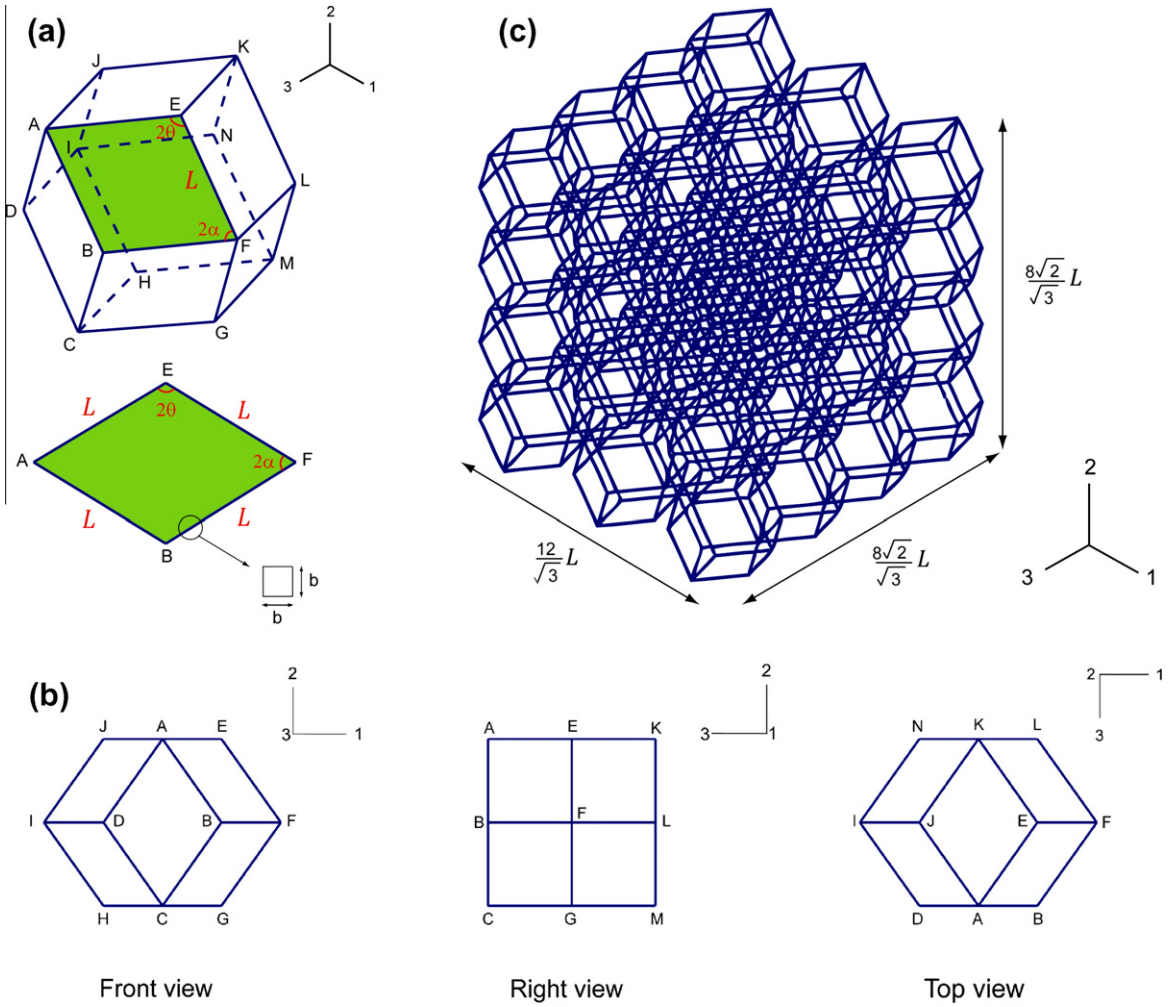

Fig. 1. Schematic of a regular rhombic dodecahedron structure. (a) A rhombic dodecahedron unit cell comprises 12 identical rhombuses, with edge length L and constant angles $2\alpha \approx 70.53^\circ$ and $2\theta \approx 109.47^\circ$. In this figure, the top and bottom surfaces (denoted by AJKE and CHMG) are perpendicular to axis 2. The front and back surfaces (denoted by ABCD and KLMN) are perpendicular to axis 3. The line connecting points I and F is in the direction of axis 1. (b) A rhombic dodecahedron unit cell in different views. Due to symmetry in directions 2 and 3, the top and front views of the unit cell are identical. (c) A tessellated rhombic dodecahedron cellular structure with 66 unit cells. The dimensions of the model relative to the cell edge length of one unit cell are shown in the picture.

Cellular structures with a similar structural organization are observed in nature. Honeybees use the geometry of a rhombic dodecahedron to form a honeycomb from a tessellation of cells, each of which is a hexagonal prism capped with half a rhombic dodecahedron. Some minerals, such as garnet, have a rhombic dodecahedral crystal habit. The rhombic dodecahedron also appears in the unit cells of diamond and diamondoids [50]. Recently, the formation of rhombic dodecahedral particles of C70 has been also observed [51].

In Section 2, we present analytical models to calculate the effective elastic–plastic properties of a rhombic dodecahedron unit cell and periodic tessellated cellular structure. The cell edge material behavior was taken as elastic–perfectly plastic, and comprised the elastic modulus, E_s, yield strength, σ_{Ys}, and Poisson's ratio, v. Our analytical models give estimates of the effective elastic moduli, Poisson's ratios, yield strengths and buckling strengths for loading along three orthogonal axes, as shown in Fig. 1. In Section 3, we construct finite element models of the cellular structures. The comparison between the finite element results and the analytical predictions are presented in Section 4. In Section 5, we develop finite element models of irregular rhombic dodecahedron cellular structures, which are subsequently used to investigate the role of irregularity in determining the basic mechanical properties of cellular structures. The irregularity was induced in the cell edge organization of the structure by randomly moving the vertices of the regular structure in three directions to create cellular structures with different cell sizes (polydisperse foams). Finally, in Section 6, we analyze the mechanical properties of the cellular structures attached to two rigid plates. This part of the work was carried out in view of recent interests in developing novel lightweight and multifunctional sandwich structures with low-density core constructions [52,53]. We show that a cellular structure attached to rigid plates is significantly stiffer compared to the counterpart structure with a periodic boundary condition, and its effective elastic modulus ~ density. Conclusions are drawn in Section 7.

2. Analytical predictions for fundamental mechanical properties

In this section, we derive analytical relationships for the effective mechanical properties of an open rhomboidal dodecahedron unit cell and tessellated cellular structure with periodic boundary conditions using fundamental concepts of mechanics of materials (assuming small deformations). E_i and σ_{Yi} denote the effective elastic modulus and effective yield strength of the cellular structure in three orthogonal directions ($i = 1, 2, 3$). In each loading direction, we also obtained the Poisson's ratios in the two directions normal to loading. The Poisson's ratio is denoted by v_{ij}, where i is the loading direction and j is the direction normal to loading (e.g. for loading in $i = 1$, we calculated v_{12}, v_{13}). It should be noted that the cellular structure under study has three orthogonal planes of symmetry and is orthotropic. Due to symmetry, the mechanical properties in directions 2 and 3 are identical (i.e. $E_2 = E_3$, $\sigma_{Y2} = \sigma_{Y3}$, $v_{12} = v_{13}$, $v_{21} = v_{31}$, $v_{23} = v_{32}$).

2.1. Elastic modulus and Poisson's ratio in direction 2 or 3

Fig. 2a shows the deformed configuration of a rhombic dodecahedron unit cell with 24 cell edges (beams) subjected to uniaxial compression, F_2 in direction 2. To obtain the effective elastic modulus of the unit cell, we calculated the relative displacement of the top and bottom rhombic faces, as the unit cell is subjected to uniaxial compression imposed by two rigid plates at the top and bottom of the unit cell. Eight cell edges that construct the top and bottom rhombic faces are considered to be in contact with the rigid plates, and thus do not contribute to the mechanical response of the unit cell. Moreover, the four cell edges located in the mid-plane cell of the unit cell are neither bent nor stretched during compression and only undergo translational rigid body motion in direction 1 (and thus do not contribute in stiffness). Six linkages, denoted by ABC, EFG, KLM, KNM, JIH and ADC in Fig. 2a, have equal contribution in the mechanical response of the unit cell in direction 2, and thus it is adequate to just analyze the response of one linkage (e.g. ABC shown in Fig. 2b). This pair of cell edges is subjected to force $P = F_2/6$ in direction 2 and moment M, which tends to bend the cell edges. The moment can be calculated using Castiglione's theorem, $M = PL\cos\theta/2$. The deflection of the unit cell in direction 2 can be obtained using Euler–Bernoulli beam theory. Ignoring the shear strain energy gives $\delta_{22} = PL^3\cos^2\theta/12E_sI + PL\sin^2\theta/E_sA$, where I and A denote the second moment of inertia and the area of the beam cross-section, respectively, and $\theta = 54.73°$. The strain in direction 2 is $\varepsilon_{22} = \delta_{22}/L\sin\theta$ and the applied stress in the same direction is $\sigma_2 = F_2/4L_2\sin 2\theta$, where the effective area is assumed at the mid-height of the unit cell. The effective elastic modulus of the unit cell parallel to direction 2 is $E_{2u} = \sigma_2/\varepsilon_{22}$, which gives

$$\frac{E_2u}{E_s} = \frac{27\sqrt{3}}{\frac{L^4}{I} + \frac{24L^2}{A}} = \frac{3}{3\sqrt{3} + \rho}\rho^2 \approx \rho^2/\sqrt{3} \cong 0.58 \tag{1}$$

The cell edges mainly deform in bending, and the contribution of the stretching stiffness of the cell edges in the overall stiffness is negligible.

For a 3-D rhombic dodecahedron cellular structure, each cell edge is shared amongst three unit cells and the effective elastic modulus decreases with increasing number of unit cells. The lower limit for the elastic modulus of a tessellated cellular structure, E_2, is 2/3 of the elastic modulus of the unit cell, which is achieved for a cellular structure of infinite size. In this case,

$$\frac{E_2}{E_s} \cong \frac{2}{3\sqrt{3}}\rho^2 \cong 0.38\rho^2 \tag{2}$$

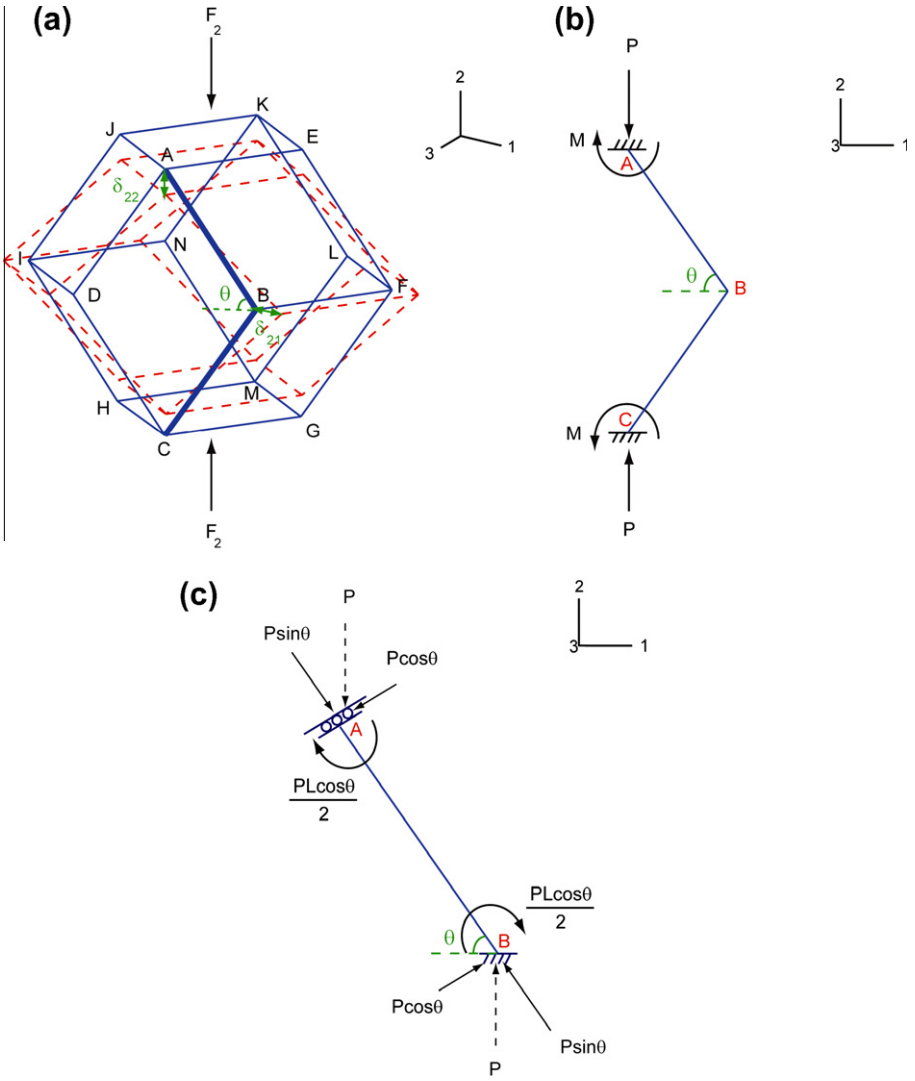

Fig. 2. (a) Schematic of a rhombic dodecahedron unit cell under uniaxial compression in direction 2. The deformed and undeformed shapes are shown by dashed and solid lines, respectively.δ_{22} is the displacement of the nodes located on the top surface of the unit cell. δ_{21} is the displacement of the nodes located in the mid-plane of the unit cell in direction 1 due to the uniaxial compression in direction 2. (b) Free body diagram of linkage ABC. (c) Free body diagram of cell edge AB.

To calculate v_{21}, we applied the Castiglione's theorem to find the displacement in direction 1 as the 3-D tessellated cellular structure is subjected to compression in direction 2. This gives $\delta_{21} = PL^3 \sin 2\theta/48E_sI - PL\sin 2\theta/4E_sA$. The strain in direction 1 due to uniaxial loading in direction 2 is $\varepsilon_{21} = \delta_{21}/L\cos\theta$ and the Poisson's ratio is $v_{21} = -\varepsilon_{21}/\varepsilon_{22}$. By ignoring the axial deformation terms for δ_{22} and δ_{21} (i.e. the second terms in the above equations), $v_{21} = 1$. Similar calculation of the Poisson's ratio in direction 3 under loading in direction 2 yields $v_{23} = 0$.

2.2. Elastic modulus and Poisson's ratio in direction 1

The analytical solution for the elastic properties of a rhombic dodecahedron unit cell shown in Fig. 2a subjected to uniaxial compression in direction 1 is presented in the Appendix A. This geometrical unit cell cannot be used to obtain the mechanical properties of the tessellated cellular structure in direction 1, as its deformation does not represent the response of a 3-D rhombic dodecahedron cellular structure of infinite size. For a tessellated structure, the analytical solution will be different from the geometrical unit cell and is remarkably straightforward. The tessellated structure shown in Fig. 3a can be divided into segments shown in Fig. 3b with identical deformation. Thus, the analysis of the segment shown in Fig. 3b is sufficient. In Fig. 3b, $C = F_1/4 = \sigma_1 A_1/4$, where $A_1 = 4L^2\sin^2\theta$ is the effective cross-section area in direction 1 and σ_1 is the applied stress in direction 1. The four cell edges shown in Fig. 3b have equal values of strain energy, and thus the total strain energy of the segment is

$$U_1 = 4\int_0^L M^{*2}/2E_sIdx_s + 4\int_0^L N^{*2}/2E_sAdx_s$$

where $M^* = -M + \sqrt{2}Cx_s/2\sqrt{3}$ and $N^* = -C/\sqrt{3}$ and $0 \leqslant x_s \leqslant L$ is the distance from one end of the cell edge, as shown in Fig. 3b. Analogous to the calculation presented in the Appendix A for the rhombic dodecahe-

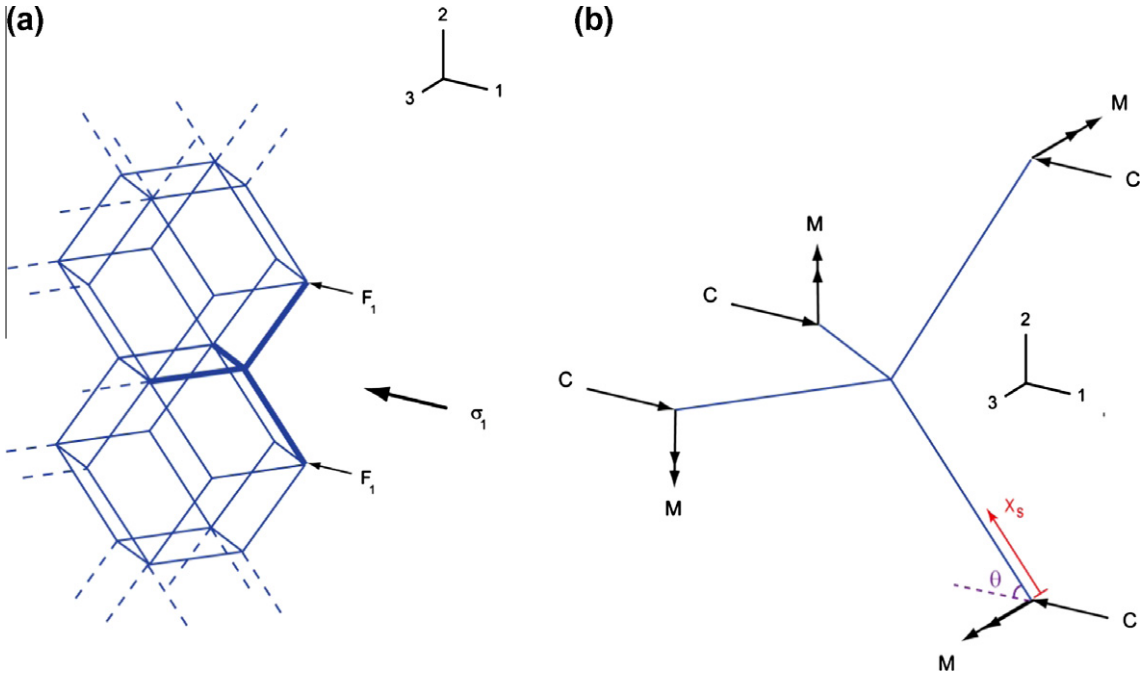

Fig. 3. (a) Schematic of a tessellated rhombic dodecahedron cellular structure under uniaxial compression in direction 1. (b) Free body diagram of the tessellated structure.

dron unit cell, minimizing the total strain energy in respect to M gives $M = \sqrt{2}Cx_s/2\sqrt{3}$ and application of the Castiglione's theorem gives $\delta_{11} = CL^3/9E_sI$. Thus, the effective elastic modulus of a 3-D rhombic dodecahedron cellular structure in direction 1 is

$$\frac{E_1}{E_s} = \frac{1}{3\sqrt{3}}\rho^2 \cong 0.19\rho^2 \tag{3}$$

which is half of its effective elastic modulus in directions 2 and 3 (i.e. $E_1 = E_2/2$). E_1 is 29.14% smaller than the effective elastic modulus of the unit cell in the same direction, which is obtained in the Appendix A. The Poisson's ratios, v_{12} and v_{13}, for a tessellated rhombic dodecahedron cellular structure can be obtained using the basic relationship for an orthotropic material ($v_{12}/E_1 = v_{21}/E_2$, $v_{31}/E_3 = v_{13}/E_1$), which gives $v_{13} = v_{12} = 0.5$. It should be noted that v_{12} and v_{13} can also be calculated using Castiglione's theorem, which gives the same result. The volume change per unit volume of the cellular structure in this loading condition is equal to the summation of the strains in three directions, which is equal to $\sigma_1(1/E_1 + v_{21}/E_2 + v_{31}/E_3) = 0$. This shows that the cellular structure is incompressible under this loading condition. A similar conclusion is valid for loading in directions 2 and 3.

2.3. Yield strength

The proportional limit (elastic limit) stress of a unit cell, denoted here by σ_{pli}, where i is the direction of loading, is the maximum stress where the relationship between the stress and strain (or equivalently force and displacement) is linear. The nonlinear response is initiated when the stress in one point of the cellular structure reaches the yield stress of the cell edge material, σ_{Ys}. For a unit cell shown in Fig. 2b, the maximum axial stress in the cell edges can be estimated as $\sigma_{b2} = Mb/21 + p\sin\theta/A$, where $M = PL\cos\theta/2$. The second term (contribution of P) is negligible compared to the first term for a low-density cellular structure. Ignoring the axial term and equating $\sigma_{b2} = \sigma_{Ys}$ gives $\sigma_{p12}/\sigma_{Y_s} = 3\sqrt{6}b^3/8L^3 = \sqrt[4]{3}/6\rho^{\frac{3}{2}}$. The yield strength of the unit cell in direction 2, $\sigma_{Y_{2u}}$, is approximately reached when the bending moment reaches the fully plastic moment of the cell edge cross-section. In our study, the cell edges have a square cross-section and the yield strength is 1.5 times the proportional limit stress (by ignoring the axial term). Thus,

$$\frac{\sigma_{Y_{2u}}}{\sigma_{Y_s}} = \frac{9\sqrt{3}}{8\sqrt{2}}\frac{b^3}{L^3} = \frac{\sqrt[4]{3}}{4}\rho^{\frac{3}{2}} \cong 0.33\rho^{1.5} \tag{4}$$

For an infinite size tessellated structure, the yield strength in direction 2 is denoted by σ_{Y_2} and is 2/3 of the yield strength of the unit cell,

$$\frac{\sigma_{Y_2}}{\sigma_{Y_s}} = \frac{3\sqrt{6}}{8}\frac{b^3}{L^3} = \frac{\sqrt[4]{3}}{6}\rho^{\frac{3}{2}} \cong 0.22\rho^{1.5} \tag{5}$$

For a tessellated rhombic dodecahedron cellular structure in direction 1, the maximum axial stress occurs at the two ends of each cell edge (beam), $\sigma_{b1} = Mb/2I + C\cos\theta/A$. By ignoring the effect of the axial term, equating $\sigma_{b1} = \sigma_{Y_s}$ gives $\sigma_{pl1}/\sigma_{Y_s} = \sqrt{6}b^3/4L^3 = \sqrt[4]{3}/9\rho^{\frac{3}{2}}$. Thus, the yield strength of the tessellated structure in direction 1, σ_{Y1}, can be estimated from:

$$\frac{\sigma_{Y1}}{\sigma_{Ys}} = \frac{3\sqrt{6}}{8}\frac{b^3}{L^3} = \frac{\sqrt[4]{3}}{6}\rho^{\frac{3}{2}} \cong 0.22\rho^{1.5} \tag{6}$$

Interestingly, while the cellular structure is orthotropic in the elastic regime, it has equal yield strength in all loading directions, which is almost equal to the yield strength of the open-cell tetrakaidecahedral cellular structures.

2.4. Elastic buckling strength

The critical buckling load of the unit cell shown in Fig. 2a in direction 2 can be obtained by using the classical Euler's buckling theory and applying the appropriate boundary conditions for the pair of cell edges shown in Fig. 2b. In the analysis, the transverse force $P\cos\theta$ and the moment $PL\cos\theta/2$ cause a pre-buckling transverse deformation of the cell edge and the axial load of the cell edge is $P\sin\theta$ (see Fig. 2c). The non-trivial solution for the general equation of the cell edge transverse displacement gives the critical buckling load of the cell edge, $F_{cr_2} = 6P_{cr} = n^2\pi^2E_sb^4/2L^2\sin\theta$, and $\sigma_{cr_2}/E_s = n^2\pi^2b^4/16L^4\cos\theta\sin^2\theta$. For $\theta = 54.735^\circ$ and $n = 1$ (i.e. first buckling mode), the critical elastic buckling stress of the unit cell, denoted by σ_{cr_2u}, can be estimated from:

$$\frac{\sigma_{cr_2u}}{E_s} = \frac{3\sqrt{3\pi^2}}{32}\frac{b^4}{L^4} = \frac{\pi^2}{24\sqrt{3}}\rho^2 \cong 0.24\rho^2 \tag{7}$$

For a tessellated rhombic dodecahedron structure, the critical buckling stress, denoted by σ_{cr_2}, is 2/3 of the critical buckling stress of the unit cell (similar to the elastic modulus):

$$\frac{\sigma_{cr_2}}{E_s} = \frac{\sqrt{3\pi^2}}{16}\frac{b^4}{L^4} = \frac{\pi^2}{36\sqrt{3}}\rho^2 \cong 0.16\rho^2 \tag{8}$$

The critical buckling load of the tessellated cellular structure in direction 1 shown in Fig. 3b is $F_{cr_1} = \pi^2E_sb^4/3L^2\cos\theta$ and the critical buckling stress, denoted by σ_{cr_1}, can be estimated from:

$$\frac{\sigma_{cr_2}}{E_s} = \frac{\sqrt{6\pi^2}}{16}\frac{b^4}{L^4} = \frac{\pi^2}{18\sqrt{6}}\rho^2 \cong 0.22\rho^2 \tag{9}$$

3. Finite element modeling of the 3-D cellular structure

In this section, we develop finite element models of both unit cell and tessellated cellular structures and use them to establish the validity of the analytical models presented in Section 2. The simulations were carried out using the finite element package Abaqus (SIMULIA, Providence, RI). The boundary condition for the unit cell model is straightforward and identical to the boundary condition assumed in the analytical investigations. For loading in each direction, two rigid plates were attached to the opposite ends of the cellular structure and displaced towards each other in the simulations. For a tessellated cellular structure, periodic boundary conditions were applied in both directions normal to the loading direction to avoid the influences of the model boundaries on the simulation results. To generate the periodic boundary conditions in a 3-D structural model, the opposite boundary planes of the model must maintain the same shape during the deformation, as shown schematically in Fig. 4. For our model (Fig. 1c), the periodic boundary condition was applied in both directions 2 and 3, when investigating the properties of the structure in direction 1. Similarly, for analyzing the mechanical properties in the direction 2, the period boundary condition was applied in directions 1 and 3. To define the above description mathematically, the following relationships have to be specified in the finite element models for each pair of nodes located on the opposite boundary planes:

$$\begin{aligned} &\theta_n^{m^+} = \theta_n^{m^-} \\ &u_n^{m^+} - u_n^{m^-} = (u_n)_{ref}^{m^+} - (u_n)_{ref}^{m^-} \quad m = 1,2,3 \text{ and } n = 1,2,3 \end{aligned} \tag{10}$$

where m^+ and m^- are the opposite boundary planes of the cellular structure (e.g. planes 1^+ and 1^-, shown in Fig. 4). $\theta_n^{m^+}$ and $\theta_n^{m^-}$ are the rotation angles and $u_n^{m^+}$ and $u_n^{m^-}$ are the displacements of the nodes on the m^+ and m^- planes in the n direction. $(u_n)_{ref}^{m^+}$ and $(u_n)_{ref}^{m^-}$ are the displacements of a pair of arbitrary reference points on the opposite boundary planes (e.g. r and r' in planes 1 and 1′, shown in Fig. 4). The second equation implies that the difference in displacements in all three directions must be equal for all pair nodes located on the opposite boundary planes [42]. Similar to the simulations for the unit cell, two rigid plates were attached to the opposite ends of the cellular structure in the loading direction and displaced towards each other in the simulations. The cell edges were allowed to move relative to the flat plates with no friction, and could freely expand in the lateral directions.

The elastic properties and yield strength of the cellular structure were calculated from the force–displacement response of the structure in each basic loading direction. The effective elastic modulus is the initial slope of the response; the Poisson's ratios were calculated by dividing the negative value of the lateral strain by the axial strain. The yield strength was obtained by plotting the stress–strain curve of the structure and finding the point at which

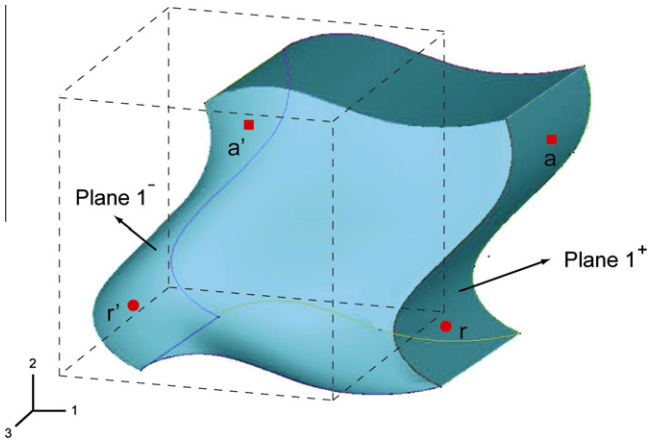

Fig. 4. Schematic of the periodic boundary conditions.

there is an increase in strain with no increase in stress (the beginning of the plateau region of the curve). The subspace eigensolver method was employed to estimate the critical elastic buckling loads of the unit cell in each loading direction. In all calculations, we assumed the cell edge material to be linear elastic–perfectly plastic, with elastic modulus $E_s = 70\,\text{Gpa}$, yield strength $\sigma_{Y_s} = 130\,\text{MPa}$ and Poisson's ratio $v = 0.3$. It should be noted that all the results are expressed in the non-dimensional form and are independent of the values of the material properties used in the calculations. The cell edges were meshed using a standard Timoshenko beam element (element type B31 in Abaqus) that uses linear interpolation (two-node linear beam) and allows for transverse shear deformation. A mesh sensitivity analysis was performed to ensure that the result is not sensitive to the mesh size. The static general solver with general (standard) contact condition available in Abaqus was used in the calculations.

4. Mechanical properties of open-cell rhombic dodecahedron cellular structures

Fig. 5a shows the finite element model of a cellular structure subjected to loading in direction 1. Fig. 5b shows the effective elastic moduli of the tessellated cellular structure in directions 1 and 2 as a function of the relative density of the tessellated cellular structure, ρ. In the finite element calculations, the relative density of the cellular structure was varied by changing the size of the square cross-section of the cell edges, b. In the same figures, we have also plotted the theoretical estimates of the effective elastic moduli in two directions from Eqs. (2) and (3). These analytical estimates are based on considering only the bending deformation of the cell edges. For cellular structures with a low relative density, the finite element and theoretical results are in good agreement, as bending is the dominant deformation mechanism. By increasing the relative density of a cellular structure, the contribution of the axial deformation of the cell edges to its overall stiffness becomes more significant and accounts for the difference between the finite element and numerical solutions. A similar comparison is made in Fig. 5c for the three different Poisson's ratios, v_{13}, v_{23}, and v_{21}, of the tessellated cellular structure, which show good agreement between the analytical predictions and the finite element results. The results suggest that the cellular structure behaves as a near-incompressible orthotropic material. Finally, in Fig. 5d we compare the finite element results and analytical predictions for the yield strength of the tessellated cellular structure in directions 1 and 2. The results show good agreement between the finite element and analytical results. The yield strength obtained from the finite element analysis is slightly higher than the analytical predictions.

To examine whether Euler buckling occurs prior to yield, we compared the critical buckling stress and the yield strength of the structure under loading in each direction. For loading in direction 2, the buckling and yield stresses equations (Eqs. (8) and (5), respectively) give the following relationship between the cell edge material yield strength and elastic modulus for the condition where Euler buckling and plastic collapsing occur simultaneously: $\sigma_{Y_s}/E_s = 0.72\rho^{0.5}$. At each relative density, yield is the dominant mode for lower values of σ_{Y_s}/E_s and buckling is dominant for higher values of σ_{Y_s}/E_s. The same approach for loading in direction 1 yields $\sigma_{Y_s}/E_s = 1.02\rho^{0.5}$. These critical limits are plotted in Fig. 6, which shows the predicted collapse mechanism in each region of the plot for each loading direction. For almost all open-cell tessellated rhombic dodecahedron structures, yielding precedes Euler buckling since generally $\sigma_{Y_s}/E_s < 0.01$.

5. Role of irregularity in the structural organization

Numerical simulations of the mechanical properties of 3-D open-cell structures with regular, irregular and random structural arrangements have been carried out by several groups [32–34]. Roberts and Garboczi [54] used a finite element method to predict the Young's modulus and Poisson's ratio of four realistic random models of isotropic open cellular solids. They proposed different relationships for low- and high-density open-cell cellular structures, and compared their results with experimental data. Elsewhere [55,56], the tensile elastic properties of a regular dodecahedron with pentagonal faces were studied to gain insight into the mechanical behavior of lungs. Here, we develop finite element models of irregular 3-D rhombic dodecahedron cellular structure to study the role of irregularity on the mechanical properties of tessellated cellular structures. Specifically, we develop models with irregular cellular organizations by perturbing the locations of the vertices of a rhombic dodecahedron structure, which leads to models with various cell sizes (polydisperse foam; Fig. 1c). In developing the models, the vertices of the cellular structure located on the boundaries are fixed and the periodic boundary conditions are applied in two directions in each model, as described in the previous section. In generating each model of the irregular structure, the vertices of a regular structure not located on the boundary are perturbed randomly according to:

$$\overline{X}_j = X_j + \gamma L \omega_j, \quad \text{for } j = 1, 2, 3 \tag{11}$$

where X_j and $\overline{X}_j$ are coordinates of the vertices in the initial regular and final irregular structures, respectively. $0 \leqslant \gamma \leqslant 1$ is a parameter used to quantify the degree of cell shape irregularity, called the "irregularity index", and $-1 < \omega_j < 1$ is a normally distributed random number. The geometrical characteristics of the cellular structure, such as the number of edges, vertices and cells, remain the same in regular and irregular structures, but the rhombuses of the structure become irregular quadrilaterals. We developed a MATLAB (Mathwork, Inc., Natick, MA) code to generate models of irregular cellular structure with different irregularity indexes. The models were imported into Abaqus, similar to in Section 3, and the mechanical

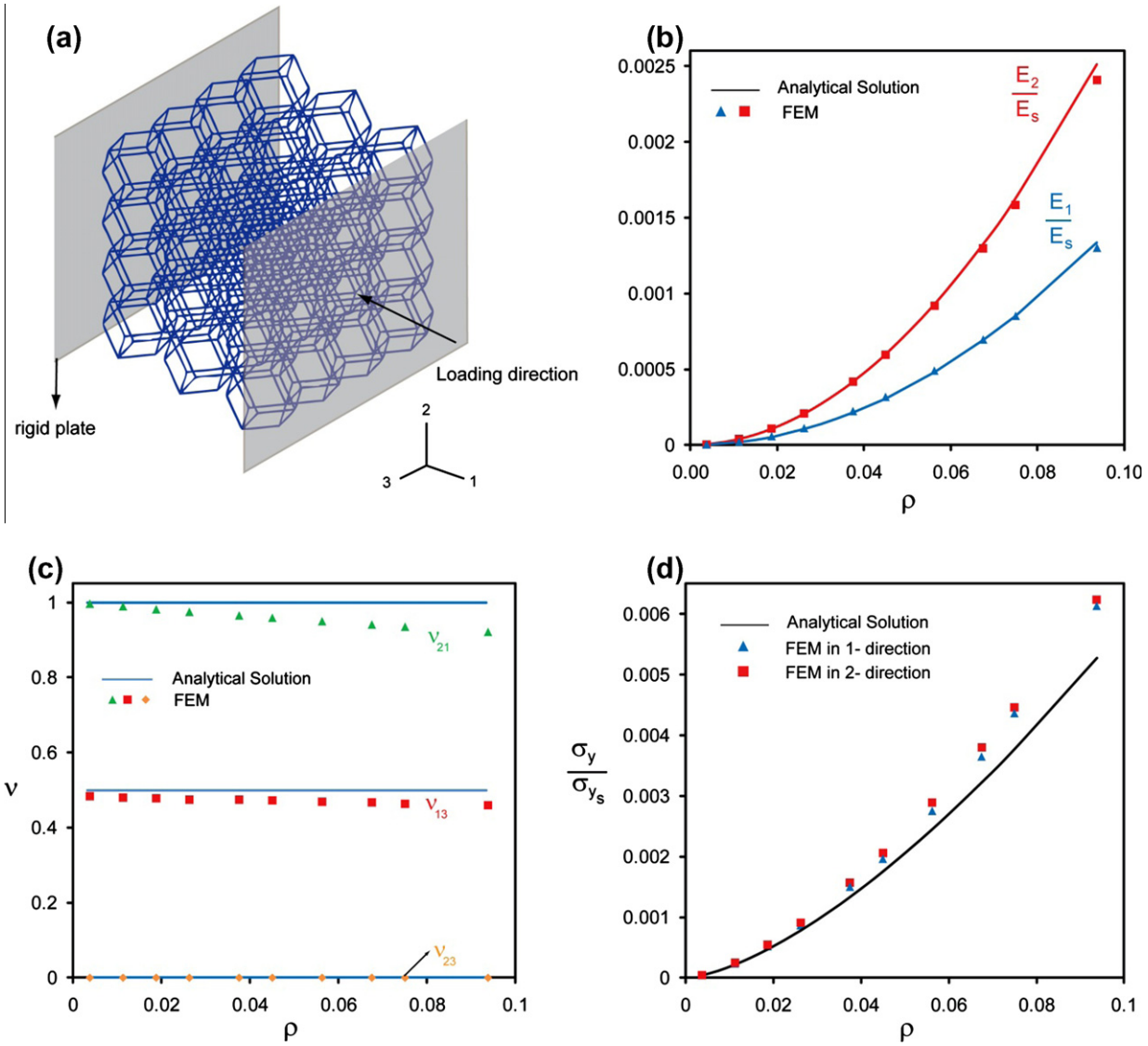

Fig. 5. Mechanical properties of the rhombic dodecahedron tessellated cellular structure. (a) Schematic of the finite element model of a tessellated structure under uniaxial compression in direction 1. (b) Normalized elastic modulus of the tessellated cellular structure vs. its relative density in directions 1 and 2. (c) Poisson's ratios of the cellular structure against its relative density. (d) Normalized yield strength of the tessellated structure vs. the relative density. The finite element results are presented for loading in both directions. The analytical prediction is identical for loading in each direction.

properties of the models were studied under loading in different directions. Fig. 7 shows three examples of the developed models with different irregularity indexes.

In this section, finite element models of irregular cellular structures with different irregularity indexes, $0 \leqslant \gamma \leqslant 0.5$, were created and analyzed. The comparison between the mechanical behavior of the regular and irregular cellular structures was made at a constant overall relative density. The total length of the cell edges varies from one model to another, and the thickness was calculated for each model to keep the overall (average) relative density the same as the regular cellular structure. For irregular cellular structures with $\gamma = 0.1$, 0.2 and 0.3, three different models of the cellular structures were constructed and analyzed. For $\gamma = 0.4$ and 0.5, we analyzed five models, since the scatter in the calculated mechanical properties is relatively large. The estimated effective elastic modulus and yield strength of the irregular structures were normalized with respect to the effective elastic modulus and yield strength of their regular cellular structure counterpart (i.e. with the same relative density). The normalized effective elastic moduli in directions 1 and 2 are denoted by $\overline{E}_1$ and $\overline{E}_2$, respectively, and the normalized yield strengths are denoted by $\bar{\sigma}_{y_1}$ and $\bar{\sigma}_{y_1}$, respectively. For a regular cellular structure, all these parameters are equal to 1. The results are summarized in Fig. 8, where the dashed lines show the average results of the finite element calculations for cellular structures at each relative density. The results show a significant decrease in yield strength and an increase in the effective elastic modulus of the structure with increasing irregularity index, γ. In general, the role of irregularity on the mechanical properties of the cellular structure is more pronounced for cellular

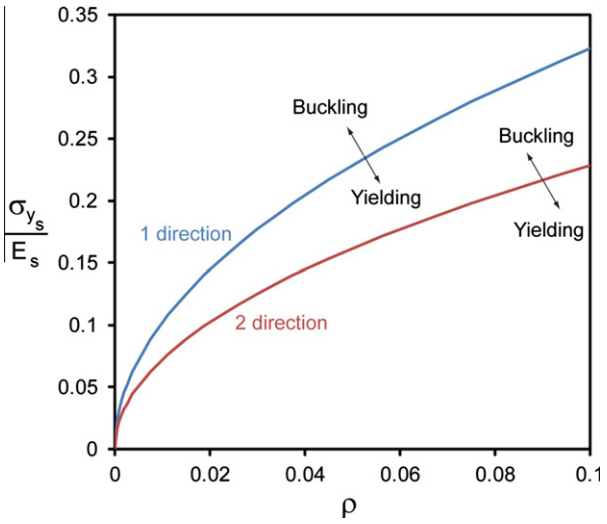

Fig. 6. Predicted collapse behavior of tessellated cellular structure for uniaxial loading in directions 1 and 2.

structures with a low relative density. Moreover, the mechanical properties in direction 2 appear to be more sensitive to the irregularity than those in direction 1.

6. Cellular structure tied to rigid plates (sandwich panel configuration)

We carried out a similar set of analytical and numerical analysis for a rhombic dodecahedron cellular structure with rigid plates attached at its two ends (the plates were normal to the loading direction and the cell edges were tied to the rigid plates). We assumed that the cellular structure is infinite in both in-plane directions. In this case, the mechanical properties of the structure are height dependent. We derived analytical estimates of the elastic modulus of the cellular structure in two extreme cases: (i) a cellular structure with a single cell height and (ii) a cellular structure with infinite height. The analytical model and the finite element calculations are discussed only briefly, as many of the details are similar to those in the previous sections.

Fig. 9 shows two segments of the structure (denoted by S1 and S2 and shown in Fig. 9a and b, respectively) that were analyzed to obtain the analytical solution for the elastic modulus of a single cell height tessellated cellular structure. All the nodes of segment S1 can only move in the loading direction (direction 2) due to symmetry. For segment S2, nodes A, B, C and D can move only in direction 2 and node E can move in both directions 1 and 2. The reaction forces and moments for each segment can be calculated by minimizing the total strain energy. For both segments, minimizing the total strain energy of the segment shows that the internal bending moment at each cross-section of all cell edges is zero. Thus, the cell edges undergo only stretching under loading in direction 2. Using the Euler–Bernoulli beam theory and ignoring the shear strain energy, the deflection of the structure in direction 2 can be obtained for each. For S1, $\delta_{22} = 3Q'L/2E_sA$, and for S2, $\delta_{22} = 3QL/2E_sA$, where Q' and Q are the compression force applied to nodes C and D of S1 and S2, respectively, as shown in Fig. 9.

The single cell height structure consists of two S1 and two S2 segments. Thus, the total resisting force of the unit cell is equal to $2Q + 2Q'$, and the effective elastic modulus of the structure is

$$\frac{E_2}{E_s} = \frac{\sqrt{3}}{4}\frac{b^2}{L^2} \cong \frac{1}{6}\rho \tag{12}$$

For the tessellated cellular structure with infinite height, the response only relates to the deformation of S2, and the total resisting force of the unit cell is equal to $4Q$. The elastic modulus of the structure can be estimated from

$$\frac{E_2}{E_s} = \frac{\sqrt{3}}{6}\frac{b^2}{L^2} \cong \frac{1}{9}\rho \tag{13}$$

Since the structure only deforms in stretching and the cell edges behave effectively as truss elements, their bending moments and deformations are mini and the elastic modulus is scaled linearly as a function of relative density. Finite element calculations were performed for 1, 2, 4 and 12 cells high structures. The periodic boundary condition was

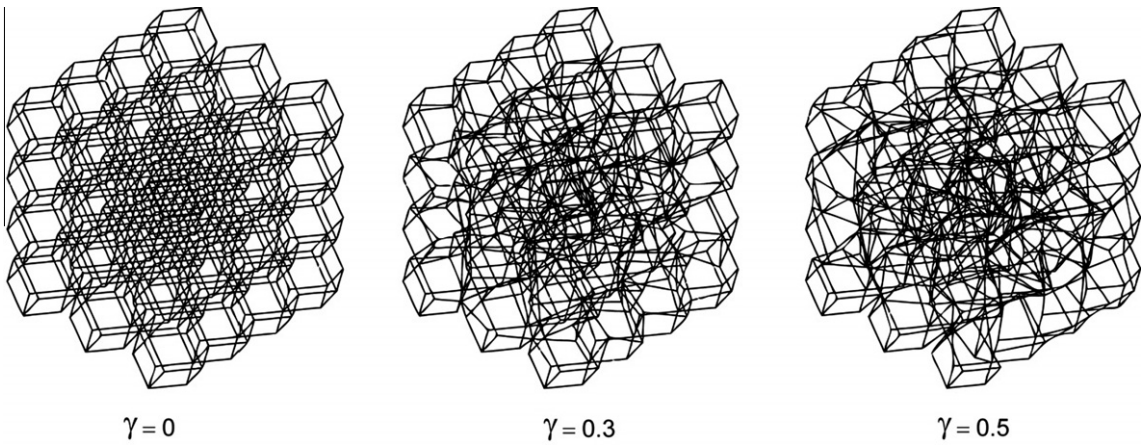

Fig. 7. Irregular cellular structures with different irregularity indexes γ.

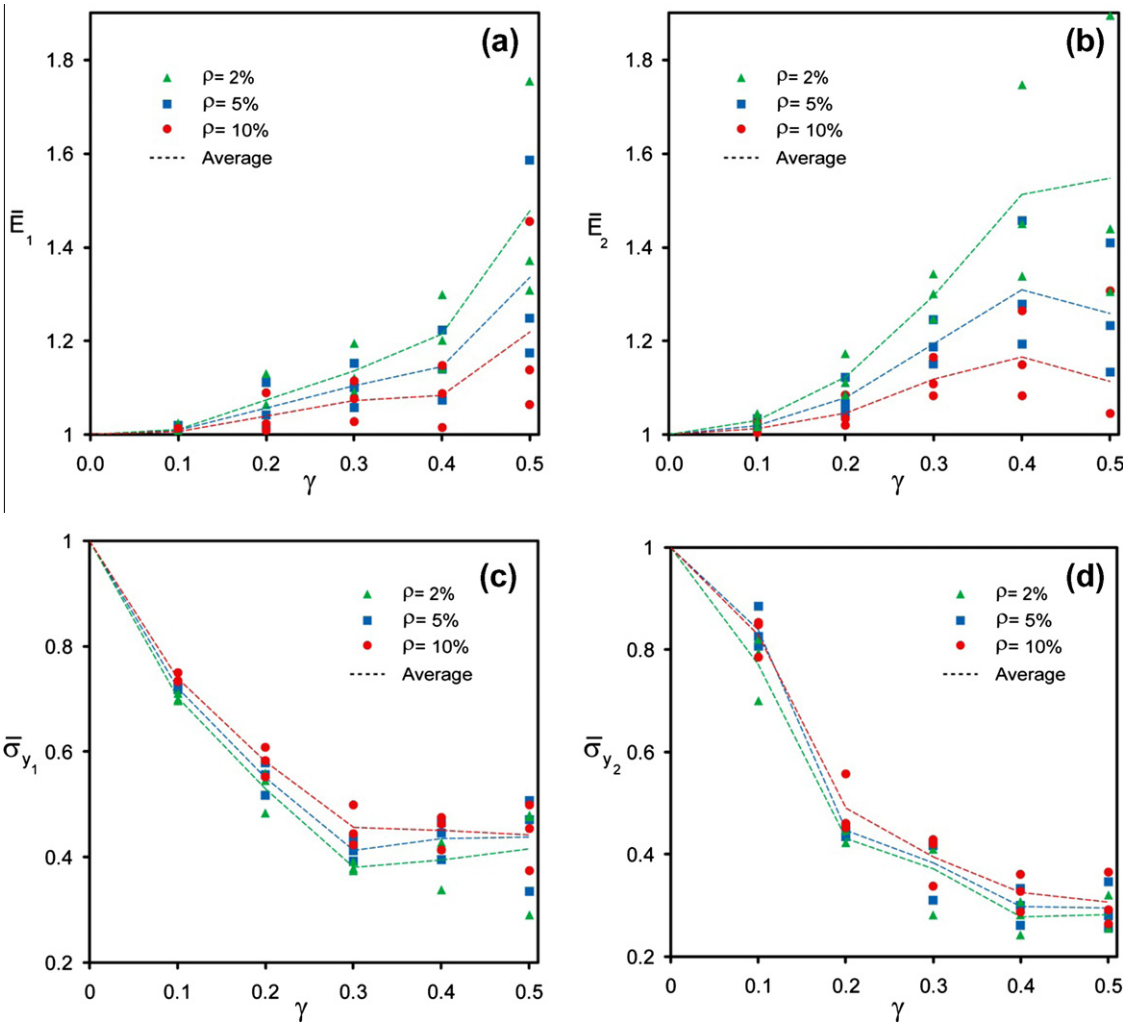

Fig. 8. Mechanical properties of an irregular cellular structure. (a and b) Normalized elastic modulus of irregular cellular structure vs. the irregularity index γ for three different relative densities in loading in directions 1 and 2, respectively. The dashed lines show the average results for each relative density. (c and d) Normalized yield strength of the irregular structure vs. the irregularity index in loading in directions 1 and 2, respectively. The dashed lines show the average results for each relative density.

applied in both directions normal to the loading direction. Fig. 10 shows the theoretical and finite element results for the elastic modulus of the cellular structure in direction 2. The solid lines represent the analytical estimates for the elastic moduli of the single cell high and infinite height structures. The results validate the descending trend of the elastic modulus with increasing height of the structure. In general, the cellular structure with tied boundary conditions is much stiffer and stronger compared to the cellular structure with the boundary condition studied in the previous sections.

7. Concluding remarks

We have provided analytical estimates for the effective elastic moduli and yield strength of 3-D Voronoi tessellation of a face-centered cubic structure called a rhombic dodecahedron in three different normal loading directions. Detailed finite element calculations were carried out to establish the validity of the analytical models. The cellular structure is twice as stiff in directions 2 and 3 as in direction 1, and is near-incompressible in all loading directions. The yield strength of the cellular structure was identical in all loading directions, indicating that yielding in direction 1 occurs at a strain that is twice the yield strain in directions 2 and 3. Comparison between the buckling load and the yielding of the cellular structure showed that for almost all open-cell tessellated rhombic dodecahedron structures, yielding precedes Euler buckling. This would suggest that the cellular structure has a similar energy absorption capacity under different loading directions if the loading is applied quasi-statically. However, under dynamic loading, the inertia effect and the contact between the cell edges could influence the energy absorption capacity of the cellular structure in different directions [5,31,53]. We also extended our study to cellular structures with a tied boundary condition (attached to rigid plates) and showed that the deformation of the cellular structure is dominated by cell

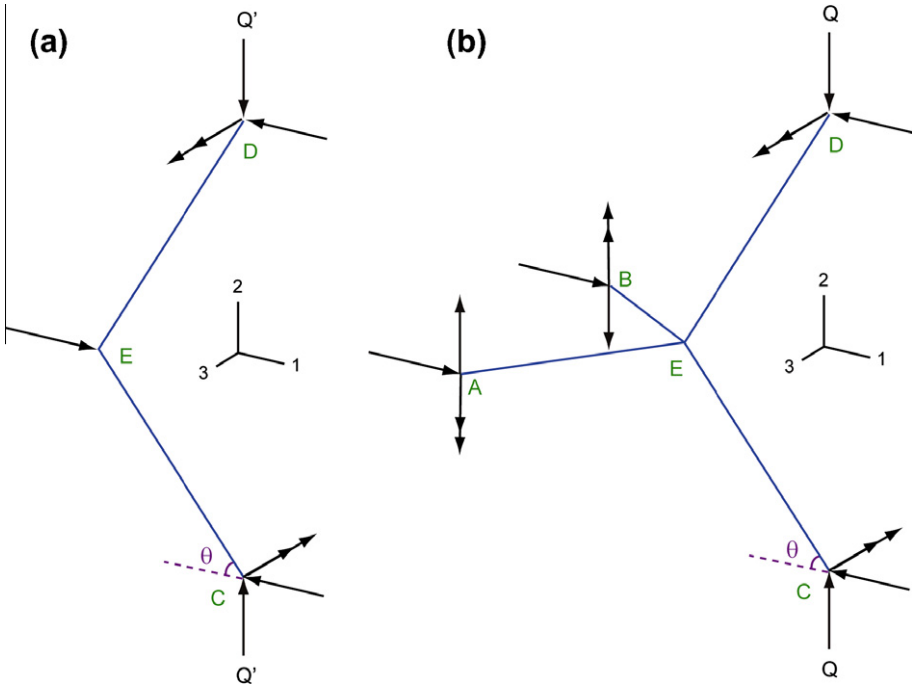

Fig. 9. Free body diagram of two segments of a rhombic dodecahedron tessellated structure tied to rigid plates under uniaxial loading in direction 2. (a and b) Free body diagrams of segments S1 and S2, respectively. The reaction forces and moments applied to each node are shown.

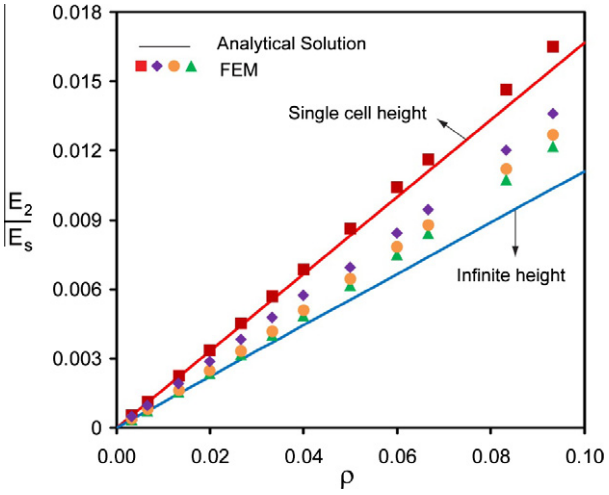

Fig. 10. Normalized elastic modulus of a rhombic dodecahedron tessellated cellular structure tied to rigid plates vs. its relative density. The analytical estimates for structures with a single cell height and an infinite height are shown by solid lines. The finite element results for structures 1, 2, 4 and 12 cells high are shown with square, rhombus, circle and triangle markers, respectively.

wall stretching. In this case, the elastic modulus of the cellular structure is a linear function of its relative density and is height dependent. In general, this cellular structure tied to rigid plates is much stiffer compared to the counterpart cellular structure with the periodic boundary condition.

The effect of irregularity in cell arrangements was also investigated. This showed an increase in the effective elastic modulus and a considerable decrease in the yield strength of the cellular structure with increasing level of irregularity in the structural arrangement of the cell edges of the cellular structure. Our results are in qualitative agreement with the results provided by Zhu et al. [57] and Van der Burg et al. [58] on the effects of cell irregularity on the elastic properties of 3-D open-cell random Voronoi foams. Moreover, the microstructure irregularities in stochastic Voronoi structures is shown to slightly elevate the effective elastic modulus and decrease the compressive strength [59]. Ajdari et al. [30] also show that two-dimensional low-density Voronoi structures are stiffer and have lower yield strength compared to a regular hexagonal honeycomb. Similar observations for the elastic properties of two-dimensional irregular honeycombs were also reported by Li et al. [60] and Silva et al. [35]. Based on the available literature, the type of irregularity appears to be a critical factor affecting the mechanical properties of heterogeneous cellular structures. Further studies are needed to systematically explore the role of irregularity type on the behavior and function of cellular structures.

Acknowledgements

We thank John W. Hutchinson and Jim Papadopolous for fruitful discussions. This work was supported in part by the US Department of Homeland Security under Award Number 2008-ST-061-ED0001 and in part by the US Air Force Office of Scientific Research under AFOSR YIP Grant Award #FA 9550-10-1-014. The views and conclusions contained in this document are those of the authors and should not be interpreted as necessarily representing the official policies, either expressed or implied, of the US Department of Homeland Security or AFOSR.

Appendix A. Mechanical properties of the geometrical unit cell in the direction 1

Fig. S1a shows the deformed configuration of a rhombic dodecahedron unit cell subjected to uniaxial compression, F_1, in direction 1. The following linkages – each consisting of three cell edges connected at one point to each other – have identical deformation and response under this loading: AEKF, KJAI, CGMF, CHMI, ABCF, ADCI, KLMF and KNMI. Thus, we analyzed the deformation of one of the linkages, as shown in Fig. S1b. The force exerted to this linkage is $R_1 = F_1/4$. The total strain energy stored in this part of the unit cell is $U_1 = U_A + 2U_B$, where U_A and U_B are the strain energy stored in cell edges EF and AE (or EK), respectively. $U_1 = U_1(R_1, R_2, R_3, M_1, M_2, M_3, M_4)$, where R_2 and R_3 are the reaction forces and M_1, M_2, M_3 and M_4 are the reaction moments applied at the boundary in Fig. S1b. Using the Euler–Bernoulli beam theory and ignoring the shear strain energy, the strain energy of cell edge EF can be estimated from

$$U_A = \int_0^L \frac{M_{A_s}^2}{2E_sI}dx + \int_0^L \frac{N_A^2}{2E_sA}dx \tag{A1}$$

where N_A and M_{A_s} are the axial force and the internal moment around axis 3. From equilibrium, $N_A = -R_1/\sqrt{3} - \sqrt{2}R_2/\sqrt{3}$ and $M_{A_s} = M_4 - \sqrt{2}R_1x/\sqrt{3} + R_2x/\sqrt{3}$, where x is the distance measured from the end of the cell edge where the external force is applied ($0 \leqslant x \leqslant L$). To calculate U_B, we used a local coordinate system ($1'2'3'$), where axis $3'$ is in the direction of the cell edge (see Fig. S1b). In this local coordinate, the total strain energy of the cell edge can be estimated from:

$$U_B = \int_0^L \frac{M_{B_{1'}}^2}{2E_sI}dx + \int_0^L \frac{M_{B_{2'}}^2}{2E_sI}dx + \int_0^L \frac{M_{B_{3'}}^2}{2G_sJ}dx + \int_0^L \frac{N_B^2}{2E_sA}dx \tag{A2}$$

where N_B is the axial force and $M_{B_{1'}}$, $M_{B_{2'}}$ and $M_{B_{3'}}$ are the internal moments applied to the cross-section of the cell edge. From equilibrium, $N_B = -R_1/2\sqrt{3} + \sqrt{2}R_3/\sqrt{3}$ and $M_{B_{1'}} = M_2 - \sqrt{2}R_1y/2\sqrt{3} - R_3y/\sqrt{3}$, $M_{B_{2'}} = -\sqrt{2}M_1\sqrt{3} + M_3/\sqrt{3} + R_2y/2$, $M_{B_{3'}} = M_1'/\sqrt{3} + \sqrt{2}M_3'\sqrt{3}$, where y is measured from the left end of the cell edge as shown in Fig. S1b ($0 \leqslant y \leqslant L$). The reaction forces and moments are unknowns, which can be calculated by minimizing the total strain energy in respect to each of them (e.g. $\partial U_1/\partial R_2 = 0$). Solving the corresponding set of equations gives:

$$\begin{aligned} R_2 &= \frac{\sqrt{2}}{6}R_1, \quad R_3 = \frac{\sqrt{2}}{12}R_1 \\ M_1 &= \frac{\sqrt{3}}{12}R_1L, \quad M_2 = \frac{7\sqrt{6}}{72}R_1L \\ M_3 &= \frac{\sqrt{6}}{24}R_1L, \quad M_4 = \frac{5\sqrt{6}}{36}R_1L \end{aligned} \tag{A3}$$

Similar to the calculations presented in Section 2.1, δ_{11} can be obtained using the Castiglione's theorem. Ignoring the strain energy associated with shear and axial deformations, $\delta_{11} = 17R_1L^3/216E_sI$. The strain in direction 1 is $\varepsilon_{11} = 2\delta_{11}/L$ and the applied stress in the same direction is $\sigma_1 = F_1/4L^2\sin^2\theta$, where the area is calculated at the middle of the cellular structure, which is a square with side length $2L\sin\theta$. The effective elastic modulus of the unit cell parallel to direction 1, $E_{1u} = \sigma_1/\varepsilon_{11}$, is:

$$\frac{E_{1u}}{E_s} = \frac{22}{81}\rho^2 \cong 0.27\rho^2 \tag{A4}$$

For a unit cell subjected to uniaxial compression in direction 1 (Fig. S1a), the maximum stress due to bending occurs at points A, E, F and K and can be estimated from $\sigma_{b1} = 5LR_1/\sqrt{6}b^3$. Equating $\sigma_{b1} = \sigma_{Y_s}$ gives $\sigma_{pl1}/\sigma_{Ys} = 3\sqrt{6}\,b^3/10L^3 = 2\sqrt[4]{3}/15\rho^{\frac{3}{2}}$. Similar to the previous section, the yield strength of the unit cell in direction 1, σ_{Y_1u}, can be estimated from:

$$\frac{\sigma_{Y_1u}}{\sigma_{Ys}} = \frac{9\sqrt{6}}{20}\frac{b^3}{L^3} = \frac{\sqrt[4]{3}}{5} \cong 0.26\rho^{1.5} \tag{A5}$$

The comparison between the analytical solution and finite element results for normalized elastic modulus and yield strength of the rhombic dodecahedron unit cell in direction 1 is shown in Fig. S1c.

Appendix B. Supplementary material

Supplementary data associated with this article can be found, in the online version, at doi:10.1016/j.actamat.2012.01.052.

References

[1] Deshpande VS, Fleck NA. J Mech Phys Solids 2003;51:187–208.
[2] Hohe J, Becker W. Appl Mech Rev 2002;55:61–87.
[3] Radford DD, McShane GJ, Deshpande VS, Fleck NA. J Appl Mech 2007;74:658–67.
[4] Vaziri A, Hutchinson JW. Int J Solids Struct 2007;44:2021–35.
[5] Vaziri A, Xue Z, Hutchinson JW. J Mech Mater Struct 2007;2(10):1947–64.
[6] Wei Z, Deshpande VS, Evans AG, Dharmasena KP, Queheillalt DT, Wadley HNG, et al. J Mech Phys Solids 2008;56:2074–91.
[7] Lu TJ, Chen C. Acta Mater 1999;47:1469–85.
[8] Vaziri A, Xue Z, Hutchinson JW. J Mech Mater Struct 2006;1(1):95–128.
[9] Evans AG, Hutchinson JW, Fleck NA, Ashby MF, Wadley HNG. Prog Mater Sci 2001;46:309–27.
[10] Famodu AA, Osadebe WC, Evans AG, Hutchinson JW, Ashby MF. Prog Mater Sci 1998;43:171–221.
[11] Gu S, Lu TJ, Evans AG. Int J Heat Mass Transfer 2001;44:2163–75.
[12] Kooistra GW, Wadley HNG. Mater Des 2007;28:507–14.
[13] Lu TJ, Stone HA, Ashby MF. Heat transfer in open-cell metal foams. Kidlington: Elsevier; 1998.
[14] Queheillalt DT, Wadley HNG. Mater Sci Eng A 2005;397:132–7.
[15] Tian J, Kim T, Lu TJ, Hodson HP, Queheillalt DT, Sypeck DJ, et al. Int J Heat Mass Transfer 2004;47:3171–86.
[16] Freyman TM, Yannas IV, Gibson LJ. Prog Mater Sci 2001;46:273–82.
[17] Hollister SJ. Nat Mater 2005;4:518–24.
[18] Hutmacher DW. Biomaterials 2000;21:2529–43.
[19] Gibson LJ, Ashby MF. Cellular solids: structures and properties. 2nd ed. Cambridge: Cambridge University Press; 1997.

[20] Gibson LJ, Ashby MF, Schajer GS, Robertson CI. Proc Roy Soc Lond Ser A, Math Phys Sci 1982;382:25–42.
[21] Hohe J, Becker W. Comput Mater Sci 2000;19:108–15.
[22] Klintworth JW, Stronge WJ. Int J Mech Sci 1988;30:273–92.
[23] Papka SD, Kyriakides S. J Mech Phys Solids 1994;42:1499–532.
[24] Torquato S, Gibiansky LV, Silva MJ, Gibson LJ. Int J Mech Sci 1998;40:71–82.
[25] Zhu HX, Hobdell JR, Windle AH. J Mech Phys Solids 2001;49:857–70.
[26] Bertoldi K, Reis PM, Willshaw S, Mullingm T. Adv Mater 2010;22:361.
[27] Lira C, Scarpa F. Compos Sci Technol 2010;70:930–6.
[28] Taylor CM, Smith CW, Miller W, Evans KE. Int J Solids Struct 2011;48:1330–9.
[29] Ajdari A, Haghpanah-Jahromi B, Papdopolous J, Nayeb-Hashemi H, Vaziri A, in press. Int J Solids Struct.
[30] Ajdari A, Nayeb-Hashemi H, Canavan P, Warner G. Mater Sci Eng A 2008;487:558–67.
[31] Ajdari A, Nayeb-Hashemi H, Vaziri A. Int J Solids Struct 2011;48:506–16.
[32] Li K, Gao XL, Subhash G. J Mech Phys Solids 2006;54:783–806.
[33] Luxner MH, Stampfl J, Pettermann HE. Int J Solids Struct 2007;44:2990–3003.
[34] Silva MJ, Gibson LJ. Int J Mech Sci 1997;39:549–63.
[35] Silva MJ, Hayes WC, Gibson LJ. Int J Mech Sci 1995;37:1161–77.
[36] Wang A-J, McDowell DL. Int J Mech Sci 2003;45:1799–813.
[37] Zhu H, Sankar BV. Compos Struct 2007;77:280–7.
[38] Ko WL. J Cell Plast 1965;1:45–50.
[39] Rosa ME, Fortes MA. Acta Crystallogr Sect A 1986;42:282–6.
[40] Thompson DW. In: Bonner JT, editor. On growth and form. Cambridge: Cambridge University Press; 1961.
[41] Weaire D, Rivier N. Contem Phys 2009;50:199–239.
[42] Jang W-Y, Kyriakides S. Int J Solids Struct 2009;46:635–50.
[43] Laroussi M, Sab K, Alaoui A. Int J Solids Struct 2002;39:3599–623.
[44] Zhu HX, Knott JF, Mills NJ. J Mech Phys Solids 1997;45:319–25.
[45] Gong L, Kyriakides S. Int J Solids Struct 2005;42:1381–99.
[46] Gong L, Kyriakides S, Jang WY. Int J Solids Struct 2005;42:1355–79.
[47] Gong L, Kyriakides S, Triantafyllidis N. J Mech Phys Solids 2005;53:771–94.
[48] Sullivan RM, Ghosn LJ, Lerch BA. Int J Solids Struct 2008;45:1754–65.
[49] Warren WE, Kraynik AM. J Appl Mech 1997;64:787–94.
[50] Webster R, Read PG. Gems: their sources, descriptions and identification. 5th ed. Oxford: Butterworth-Heinemann; 1994.
[51] Matsuoka K-I, Akiyama T, Yamada S. Langmuir 2009;26:4274–80.
[52] Xue Z, Hutchinson JW. Int J Numer Methods Eng 2004;61:2205–38.
[53] Xue Z, Hutchinson JW. Int J Numer Methods Eng 2006;65:2221–45.
[54] Roberts AP, Garboczi EJ. J Mech Phys Solids 2002;50:33–55.
[55] Budiansky B, Kimmel E. J Appl Mech 1987;54:351–8.
[56] Kimmel E, Budiansky B. J Biomech Eng 1990;112:160–7.
[57] Zhu HX, Hobdell JR, Windle AH. Acta Mater 2000;48:4893–900.
[58] Van der Burg MWD, Shulmeister V, Van der Geissen E, Marissen R. J Cell Plast 1997;33:31–54.
[59] Alkhader M, Vural M. Int J Eng Sci 2008;46:1035–51.
[60] Li K, Gao XL, Subhash G. Int J Solids Struct 2005;42:1777–95.